

Journal of
***Mechanics of
Materials and Structures***

ON THE NUMERICS AND CORRELATION OF SCRATCH TESTING

Fredrik Wredenberg and Per-Lennart Larsson

Volume 2, N° 3

March 2007



mathematical sciences publishers

ON THE NUMERICS AND CORRELATION OF SCRATCH TESTING

FREDRIK WREDENBERG AND PER-LENNART LARSSON

A numerical strategy based on the finite element method and intended for an accurate analysis of the scratch test is presented. For simplicity, but not out of necessity, the material was described by classical von Mises elastoplasticity utilizing large deformation theory. Based on this strategy numerous results are presented and correlation of scratch properties is discussed within the framework of theory for indentation testing. Furthermore, the existence of a representative plastic strain in the spirit of Tabor was studied. The investigation also concerns details regarding frictional effects, normal vs. tangential scratch hardness, similarities and differences between indentation and scratch test characteristics as well as details regarding the behavior of local field variables at scratching.

1. Introduction

Indentation testing and scratch testing show many similar features. However, due to its relative simplicity, indentation testing has been used much more frequently when, for example, material characterization is at issue. A further reason for the popularity of indentation testing is that such tests are more easily analyzed than scratch tests, and consequently a great deal of knowledge has been gained over the years regarding the mechanical behavior at indentation. Most often, at least when modern experimental devices such as the nanoindenter (or other types of instrumented indentation devices) are at issue, sharp indenters are used for practical reasons. For such indenters semiempirical relations for material characterization were derived and used by the late 1940's and early 1950's, in particular for metals and alloys [Tabor 1951]. In short, from comprehensive experimental investigations [Tabor 1951] derives a relation

$$H = C\sigma(\epsilon_{\text{repr}}), \quad (1)$$

between the indentation hardness H , here defined as the mean contact pressure at indentation, and the material yield stress at a representative value of the accumulated (effective) plastic strain ϵ_{repr} . Furthermore in Equation (1), C is a constant that only depends on the geometry of the indenter. For a Vickers indenter, Tabor [1951] determines the values $C \approx 3$ and $\epsilon_{\text{repr}} \approx 8\%$ while Atkins and Tabor [1965] find $C \approx 2.54$ and $\epsilon_{\text{repr}} \approx 11\%$ for a conical indenter with an angle of $\beta = 22^\circ$ between the indenter and the undeformed surface, as shown in Figure 1. Based partly on the above discussed results, further progress is achieved by Johnson [1970; 1985], who shows from theoretical considerations that indentation testing on different materials can be well correlated by using a parameter

$$\Lambda = \frac{E \tan \beta}{(1 - \nu^2)\sigma_{\text{repr}}}, \quad (2)$$

Keywords: scratch test, hardness, friction, finite elements, contact.

The authors acknowledge the support through grant 621-2005-5803 from the Swedish Research Council.

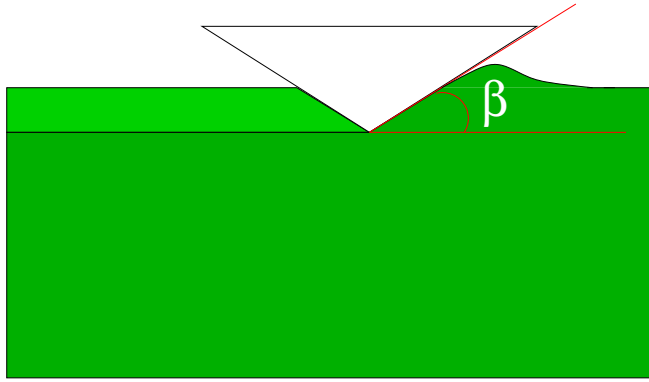


Figure 1. The angle β of a conical indenter/stylus.

where E is Young's modulus and ν is Poisson's ratio. Johnson [1970; 1985] also suggests that indentation properties for various materials will fall into one of three levels as shown in Figure 2. In level I, $\Lambda < 3$, very little plastic deformation occurs during the indentation test, and all global properties can be derived from an elastic analysis. In level II, $3 < \Lambda < 40$, an increasing amount of plastic deformation is present, and both the elastic and the plastic properties of the material will influence the outcome of a hardness test, according to Johnson [1970; 1985]. Based on the fact that the stress field just beneath the indenter in such a situation is almost hydrostatic, the process is very similar to the case of expansion of a spherical cavity in a large solid due to an internal pressure, and the formula

$$H = \frac{2}{3} \sigma_{\text{repr}} \left(1 + \ln \frac{E \tan \beta}{3(1 - \nu^2) \sigma_{\text{repr}}} \right) \quad (3)$$

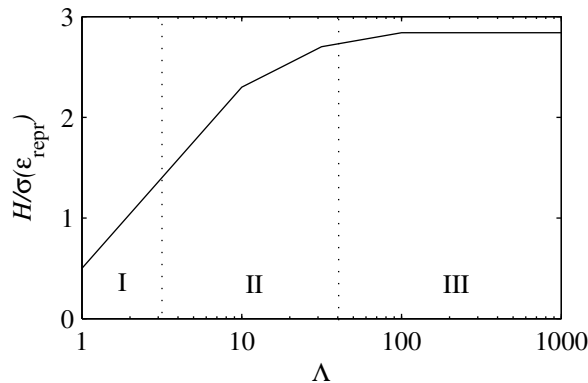


Figure 2. Sketch of the characteristic behavior of indentation hardness [Johnson 1985]. The indentation hardness H divided by the stress $\sigma(\epsilon_{\text{repr}})$ is plotted against the non-dimensional strain parameter Λ .

is derived for the hardness. Finally, in level III, $\Lambda > 40$, plastic deformation is present all over the contact area, and elasticity no longer influences the hardness value for the material. This is also the region pertinent to most standard engineering materials, such as steel and many aluminum and copper alloys, and it is also the region where Equation (1) applies.

The accuracy of the results above have been extensively tested (and improved) during the last ten to fifteen years by computational simulations of the indentation of materials with tailored constitutive properties that take advantage of modern computers and advanced numerical methods [Laursen and Simo 1992; Giannakopoulos et al. 1994; Larsson et al. 1996; Larsson 2001; Mata 2004]. In short, even though significant improvements have resulted from such numerical investigations it can be concluded that the validity of the overall findings by Tabor [1951] and Johnson [1970; 1985] have survived these scrutinizing studies. This is particularly so when it comes to such features as the existence of a representative strain at indentation, and the usefulness of the parameter in Equation (2) when it comes to correlation of indentation results [Dao et al. 2001; Larsson 2001].

Nowadays, scratch testing is also a well established technique for hardness testing. Historically, one of the earliest efforts was Mohs' hardness scale (1824), which is based on the fact a that a harder material will leave a visible scratch on a softer material if rubbed against it. The scratch test may also be used for tribological testing, although it is being questioned for use on hard coatings [Bull 1999]. Throughout the coating industry, the scratch test is used for adhesion testing of coatings. The adhesion test usually consists of a loaded diamond tip that is drawn across a surface under continuously (or stepwise) increasing load. At some load a well-defined failure occurs and the critical load is found. This technique is used for the ranking of coating adhesion.

As indicated above, the fundamental knowledge about mechanical behavior at scratching is not nearly as developed as for indentation testing. It should be mentioned, however, that early mechanical analyses concerning different aspects of scratching of metals exist and have been presented by Goddard and Wilman [1962], Childs [1970], Vathaire et al. [1981], and Gilormini and Felder [1983]. Furthermore, as the scratch test is often used to determine characteristics of polymeric coatings, this issue is also under investigation [Briscoe et al. 1996; Gauthier et al. 2001]. It goes almost without saying, however, that due to the complexity of the boundary value problem, high accuracy of results at scratch analysis can only be obtained by relying on numerical methods, preferably the finite element method (FEM). In recent years quite a few such analyses have been presented. In this context, Bucaille et al. [2001] analyze cone scratching of ideally plastic materials, and their results also indicate that the parameter Λ as given in Figure 2 can indeed be used for correlating scratch parameters as well as indentation parameters. Furthermore, Bucaille et al. [2001] find, as could be expected, that the strain levels at scratching are much higher than at indentation, but as only ideally-plastic material behavior is at issue, this finding is not explored in connection with the concept of representative strains. Further progress based on FEM analyses of the scratch test is also achieved by Bucaille et al. [2004] for polymeric materials modeled using standard elastoplasticity, corresponding to stage II rheology Figure 2.

Although beyond the scope of this work, investigations have also been performed for severe scratching, that is, fracture, delamination, and similar phenomena during scratching, by Holmberg et al. [2003], Subhash and Zhang [2002], Malzbender and de With [2001], and Thouless [1998]. Bull [1991] and others find that a coating may fail in many modes including tensile cracking, buckling and spalling. To account for the cracking behavior, Subhash and Zhang [2002] propose an *elastic-plastic-cracking* model

both for indentation and scratching. In this model the material behavior is represented by tensile cracking and compressive yielding, where a material point is assumed to fail in tension and be deleted from the model if the crack opening displacement exceeds a critical value.

From the discussion above it should be clear that the mechanical behavior at scratching is very complicated. But, based on using the finite element method, scattered progress in the understanding of different features has been gained in recent years. It remains, however, to achieve a more complete understanding of the behavior of different local and global scratch parameters, including the effect from strain-hardening, friction, and the Johnson parameter Λ . This will be attempted in the present investigation, which will also include details regarding normal versus tangential scratch hardness, similarities and differences between indentation and scratch test characteristics, as well as details regarding the behavior of local field variables at scratching. In doing so, a numerical strategy based on the finite element method, and in particular the commercial FEM package [ABAQUS 2004], was relied upon to yield results of sufficient accuracy. For clarity and convenience, but not of necessity, the analysis was restricted to cone scratching of classical elastoplastic (von Mises) materials, since in such a case no characteristic length was introduced into the problem. Scratching of thin films was not analyzed in this initial work, but will be the subject of forthcoming analyses using the present numerical scheme.

2. Theoretical background

The present analysis of scratching using a sharp conical stylus concerns a problem where quasistatic and steady-state conditions prevail. Such a situation is of substantial practical importance and is relatively easily achieved, at least during a scratch test under controlled experimental conditions. It is important to emphasize that the interpretation of the experimental scratch results then becomes much simpler.

Assuming that quasistatic and steady-state conditions prevail, as in the case of normal indentation, the problem is self-similar with no characteristic length present. Consequently, the normal hardness

$$H_{\text{norm}} = F_{\text{norm}}/A_{\text{norm}}, \quad (4)$$

and the tangential hardness

$$H_{\text{tan}} = F_{\text{tan}}/A_{\text{tan}}, \quad (5)$$

as well as a ratio h/\sqrt{A} (where h is the scratch depth), will be constant during the loading sequence of a scratch test, and stresses and strains will be functions solely of material properties and the dimensionless variable x_i/\sqrt{A} (x_i being Cartesian coordinates, as shown in Figure 3). In this context, \sqrt{A} should be interpreted as a representative contact length and the indices *norm* and *tan* represent the normal and tangential components of the scratch quantities. Clearly, the fact that the normal and tangential scratch hardness are constant during a cone scratch test is valid for classical elastoplastic material behavior, as assumed here, but it fails for strain gradient material behavior, since a characteristic length is present in the constitutive equation [Fleck and Hutchinson 1993].

Due to the characteristics of the scratch test, at least as formulated presently, a possible route of attack would be to take advantage of the prevailing steady-state conditions. Accordingly, a standard steady-state transformation converting time derivatives into spatial derivatives, as is often used to analyze crack problems, would transform the problem to a stationary one, which is certainly more attractive when a numerical analysis is at issue. However, in the present study the numerical results clearly suggest that

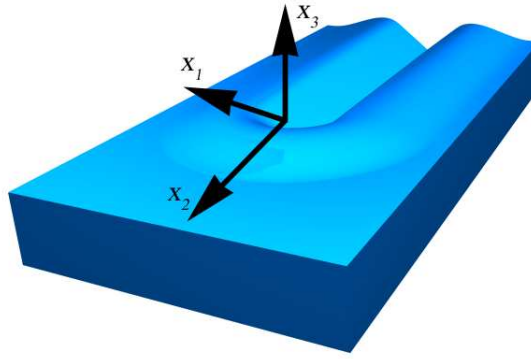


Figure 3. Cartesian coordinates x_i (following the tip of the stylus). Scratching is performed in the x_2 direction.

large deformation theory must be relied upon, and this is also the case for the corresponding normal indentation problem [Giannakopoulos et al. 1994; Larsson et al. 1996]. In addition, the strain levels at scratching are even higher, as shown by, for example, [Bucaille et al. 2001], as well as the present investigation. In such a case some of the boundary conditions resulting from a steady-state transformation become very complicated. Furthermore, the present numerical scheme will in the future be used to solve problems including film/substrate systems and in that case, steady-state conditions no longer apply. Accordingly, in the present study we relied upon a more straightforward FEM strategy, as will be discussed below.

As the constitutive specification, the incremental, rate-independent Prandtl–Reuss equation for classical von Mises plasticity with isotropic hardening is

$$\hat{\tau}_{ij} = \frac{E}{(1 + \nu)} \left(\delta_{ik}\delta_{jl} + \frac{\nu}{(1 - 2\nu)}\delta_{ij}\delta_{kl} - \frac{3\tau'_{ij}\tau'_{kl} - (E/(1 + \nu))}{2\tau_e^2\left(\frac{2}{3}K + \frac{E}{(1 + \nu)}\right)} \right) D_{kl}, \tag{6}$$

in a large strain formulation. In Equation (6), δ_{ij} is the Kronecker identity tensor, D_{ij} is the rate of deformation, and $\hat{\tau}_{ij}$ is the Jaumann rate of the Kirchhoff stress τ_{ij} . The Kirchhoff stress is related to the Cauchy stress σ_{ij} as $\tau_{ij} = J\sigma_{ij}$, where J is the ratio of volume in the current state to volume in the previous state. Furthermore, τ_e and $\hat{\tau}_{ij}$ are the von Mises effective stress and deviatoric stress, respectively. Finally, K is the instantaneous slope of the uniaxial compressive Kirchhoff stress. Note that Equation (6) is only valid at plastic loading when $\tau_e = \tau(\epsilon_p)$, the initial yield stress being given by $\tau_Y = \tau(0)$. At elastic loading or unloading, a hypoelastic formulation of Hooke’s law, pertinent to the first part of Equation (6), was relied upon. Obviously, within the present setting, kinematic hardening effects were not included in the analysis. Such effects could certainly have influenced the outcome of scratch test but would also have increased the number of required numerical computations substantially (due to an increased number of constitutive parameters) and would have made a straightforward interpretation of the results more difficult. For this reason, it was thought advisable as a first attempt to restrict the analysis to classical von Mises plasticity with isotropic hardening, especially since the loading part of a scratch test was of primary interest.

To summarize the governing equations, D_{ij} is connected with the material velocity \dot{u}_i , as

$$D_{ij} = \left(\frac{\partial \dot{u}_i}{\partial x_j} + \frac{\partial \dot{u}_j}{\partial x_i} \right), \quad (7)$$

while throughout the analysis, equilibrium equations in absence of body forces,

$$\frac{\partial \sigma_{ij}}{\partial x_j} = 0 \quad (8)$$

must be satisfied. Regarding boundary conditions, the surface outside the contact area was assumed to be traction free and within the area of contact unilateral kinematic constraints, given by the shape of the conical indenter/stylus depicted in Figure 1, and these assumptions had to be accounted for.

3. Numerical analysis

Scratching was simulated using the commercial FE-program [ABAQUS 2004] (see Figure 4 for the FE mesh). In the simulation a rigid conical stylus with attack angle $\beta = 22^\circ$ was first pressed normally into the mesh and then dragged tangentially across the surface, until steady state conditions were achieved. During the scratching process the stylus was held at a constant depth. The contact area and the reaction forces were recorded during the process. As specified above, the material was described by classical von Mises elasto-plasticity with isotropic hardening according to

$$\sigma(\epsilon_p) = \sigma_Y + \sigma_0 \epsilon_p^n, \quad (9)$$

where $\sigma(\epsilon_p)$ is the flow stress, σ_Y the initial yield stress, ϵ_p the effective plastic strain, and n the hardening exponent. The strength parameter σ_0 was adjusted so that the stress at $\epsilon_p = 8\%$ was twice that of the initial yield stress. This choice is not of importance when the numerical results are evaluated; rather, it was made by recalling the value of representative stress suggested by Tabor [1951], and it was convenient for correlating scratch/indentation results in the spirit of Johnson [1970; 1985]. As discussed above, it was found during simulations that the model experienced extremely large rotations/strains in the vicinity of the stylus. Thus, the use of large strain theory was deemed necessary.

Simulations for small values of Λ were performed with implicit time stepping and full integration elements. For larger Λ , explicit time stepping and reduced integration elements needed to be used. Full integration elements were used for small Λ to avoid the hour-glassing effect. It was also found necessary to use adaptive meshing as Λ gets larger, due to extreme element distortion. To decrease CPU time, the mesh was divided in half along the scratch, and symmetry conditions were applied. The mesh was constructed from 30284 eight node linear brick elements. These elements were chosen since they show a faster convergence with respect to mesh refinement than tetrahedral elements, and do not have the inherent contact problems of quadratic elements [ABAQUS 2004]. During the simulation some 40 elements were in contact with the stylus at any given time. The mesh domain size was $10 \times 10 \times 22.5 \text{ mm}^3$ and the scratch depth was 0.3 mm.

In Table 1 the convergence of the scratch hardness with respect to various parameters can be seen. Mass scaling was introduced to increase the time step in the explicit analysis and thus decrease the computational time. A mass scaling of 1000 was chosen for the analysis. The remeshing frequency was kept as low as possible, so as not to lose too much precision but still maintain the undistorted element

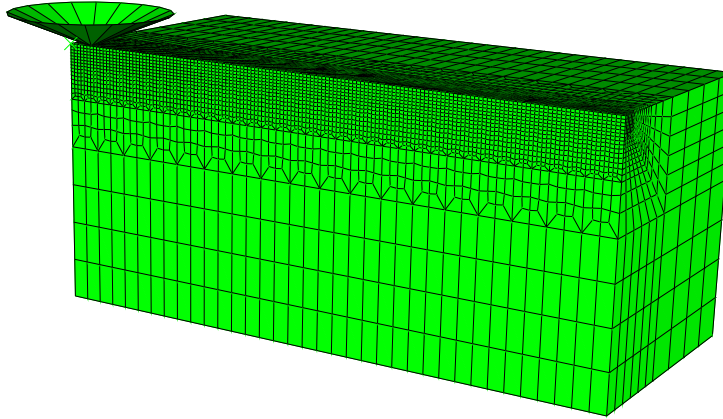


Figure 4. Finite elements mesh. Linear 8-node brick elements. Symmetry conditions apply to the surface in view. The stylus is also shown.

shape, since every remapping of the mesh causes some diffusion of the solution [ABAQUS 2004]. In Table 1 it can be seen that remeshing every 500th or 5000th time step made very little difference. The scratch depth was varied to ascertain that enough elements were in contact. Table 1 indicates that ≈ 40 elements in contact were sufficient, equaling a contact radius of approximately 1 mm. With the numerical precision secured, a parametric study was then performed for different values of Λ , n , and the interfacial coefficient of friction μ_i .

Furthermore, to simulate indentation, a finite element model developed by Larsson [2001] was used. The simulated indentation hardness, and also other indentation quantities, could then be related to the corresponding simulated scratch results.

4. Results and discussion

In this section the results from the numerical simulations are presented, and the results pertinent to the most important features related to scratching will be discussed in some detail. It should be stressed that most of the results below are pertinent to frictionless contact, but discussions about the influence

Parameter	Used	$H_{\text{norm}}/\text{MPa}$	Reference	$H_{\text{norm}}/\text{MPa}$
Mass scaling	1000	476	10000	480
Scratch depth (elements in contact)	0.3 (39)	476	0.4 (76)	472
Remeshing freq.	2e-3	476	2e-4	475

Table 1. Convergence analysis of scratch normal hardness H_{norm} at scratching, for elastic perfectly plastic material, $\Lambda = 100$.

of interfacial friction are included in each particular subchapter. Furthermore, if not stated otherwise, in most of the figures, when nondimensionalized variables are introduced, a representative stress σ ($\epsilon_p = 8\%$) was used, following Tabor [1951].

In the subchapters below, the following aspects concerning scratching and scratch testing are discussed: Section 4.1, the contact area at scratching, Section 4.2, scratch normal and tangential hardness and the concept of a representative strain, Section 4.3, the apparent coefficient of friction, and Section 4.4, scratch testing versus indentation testing. It should be mentioned that in the last subchapters the behavior of important field variables will also be discussed, and in particular those related to cracking.

4.1. The contact area at scratching. The contact area at indentation (and at scratching) is a very important parameter for material characterization, for one. Accordingly, it seems advisable to discuss this feature first of all in the context of analytical and numerical estimates, and in particular with the correlation of elastoplastic material parameters in mind.

An estimate of the normally projected contact area (A_{norm}) for large Λ is given by Goddard and Wilman [1962] as

$$A_{\text{norm}} = (w/2)^2 \frac{\pi}{2}, \quad (10)$$

where w is the scratch width (distance between the top levels of the residual groove). The tangentially projected contact area (A_{tan}) can be found through a simple geometric consideration as

$$A_{\text{tan}} = \frac{w^2}{4} \tan \beta. \quad (11)$$

These expressions are based on solely geometrical considerations, assuming that the contact area is semiconical.

In Figure 5 the actual contact area can be seen during simulation of scratching of an elastic perfectly plastic material. The corresponding ratio of the actual normally projected area, A_{real} , to the contact area estimated by Equation (10), is listed in Table 2. It is clear from Table 2 that the estimate Equation (10) worked well for large Λ materials, despite the fact that the contact areas shown in Figure 5 are not perfectly semiconical. This was indeed the case for both elastic perfectly plastic materials and strain hardening materials at stage III rheology. Not so, however, for smaller Λ , since contact then also occurred on the rear face of the stylus.

Λ ($\epsilon_{\text{repr}} = 8\%$)	10	100	1000
$n = 0$	1.39	1.10	1.10
$n = 0.1$	1.33	1.08	1.12
$n = 0.17$	1.20	1.00	1.09
$n = 0.33$	1.16	0.91	1.06
$n = 1$	1.43	1.05	0.91

Table 2. Ratio of simulated actual normal contact area to estimated normal contact area by Equation (10) for different Λ , for elastic plastic material with frictionless contact. Λ ($\epsilon_{\text{repr}} = 8\%$) = 1 yielded no measurable groove width, hence the estimate was not applicable.

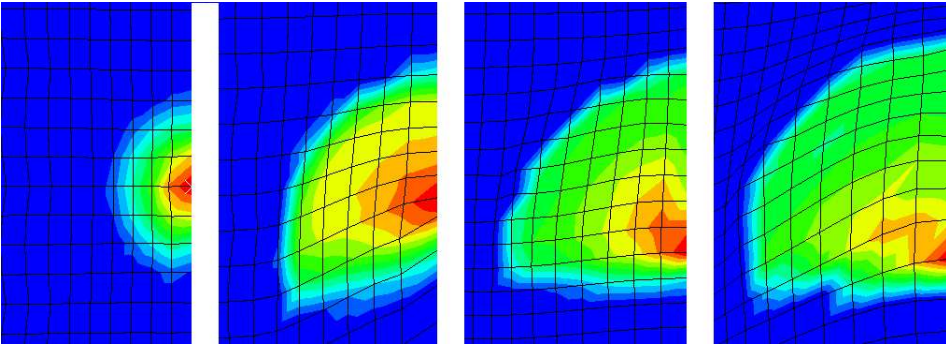


Figure 5. Contact pressure distribution at $\Lambda = 1$, $\Lambda = 10$, $\Lambda = 100$ and $\Lambda = 1000$, for elastic perfectly plastic material. Only half of the contact region is visible in the figure. The scratch direction is upwards.

Furthermore, it should be emphasized here that an estimate of the contact area based on purely geometric considerations, $A_{\text{nom}} = 1/2\pi h^2 \cot^2 \beta$, assuming a nominal semicircular normally projected contact area, is definitely not generally applicable during scratching, or during standard normal indentation testing (see Figure 6) [Larsson 2001]. It is of fundamental importance, as proven by corresponding analyses for indentation, to account correctly for piling up and sinking of material at the contact boundary when constitutive specifications are at issue. However, in this context, elastic effects are very hard to account for, and it was therefore thought advisable to present only results where rigid plasticity is dominant, as is shown in Figure 6. This figure also shows corresponding indentation results, and clearly the nominal area is far from a good approximation of the actual contact area during scratching even for predominantly plastic deformation.

4.2. Scratch normal and tangential hardness and the concept of a representative strain. In the following section the behavior of hardness values are considered. This concerns both the overall mechanical behavior and its correlation at material characterization.

In Figure 7 the scratch normal hardness is divided by the yield stress at a plastic strain level of 8% and plotted against Johnson's parameter Λ ($\epsilon_{\text{repr}} = 8\%$). It is obvious from Figure 7 that 8% was not a representative level of strain, since the curves do not coincide. Instead a different level of strain was sought. By minimizing the deviation of the curves in Figure 7 for $\Lambda(\epsilon_{\text{repr}} = 8\%) = 10, 100$, and 1000 by means of the least-squares method, a representative level of plastic strain was found. The new representative level of plastic strain was found to be approximately 35%. For $\epsilon_{\text{repr}} = 35\%$ the stress $H/\sigma(\epsilon_{\text{repr}})$ was roughly constant for large Λ materials regardless of the strain hardening exponent n (see Figure 8). Of course, this is not an obvious choice for a representative level, since, for example, Wredenberg and Larsson [2005] showed that $\epsilon_{\text{repr}} = 57\%$ could also in some cases be used (except where $n = 1$), and in addition a representative strain of 35% and 57% gives $C \approx 2.5$ and $C \approx 2.4$, respectively (see Equation (1)). It is interesting to note that in previous studies of sharp indentation problems, representative strain levels close to 35% are suggested [Larsson et al. 1996; Larsson 2001], but this corresponds to a situation where a two-parameter model (with two representative strain levels)

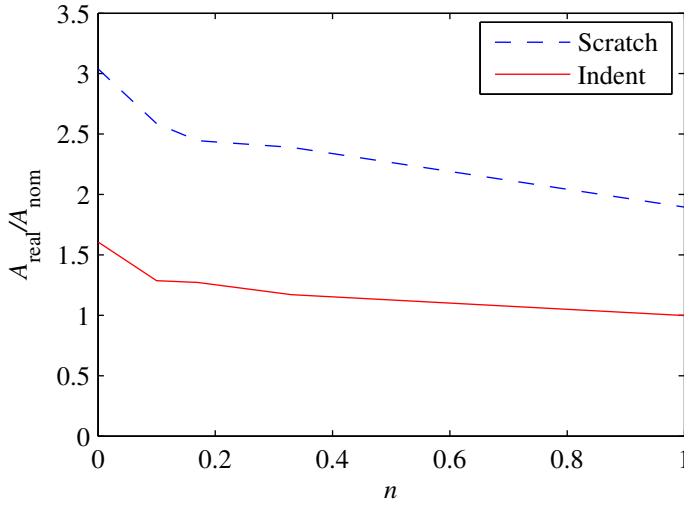


Figure 6. The actual normally projected contact area, A_{real} , divided by the nominal contact area, A_{nom} , plotted against the hardening parameter n . Results both for indentation and scratching. $\Lambda(\epsilon_{\text{repr}} = 8\%) = 1000$.

was used according to

$$H = C_1\sigma_1 + C_2\sigma_h. \quad (12)$$

In Equation (12), C_1 and C_2 are constants analogous to C in Equation (1), and σ_1 and σ_h are representative stresses at different values of the effective plastic strain. In short, it is obvious that the strain levels at scratching are significantly higher than the corresponding ones at indentation, indicating that the scratch

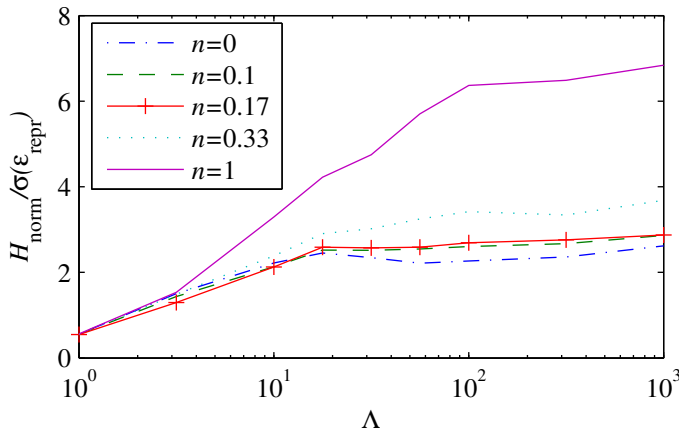


Figure 7. Scratch normal hardness divided by the yield stress, at a plastic strain of 8 %, for different $\Lambda(\epsilon_{\text{repr}} = 8\%)$ and n .

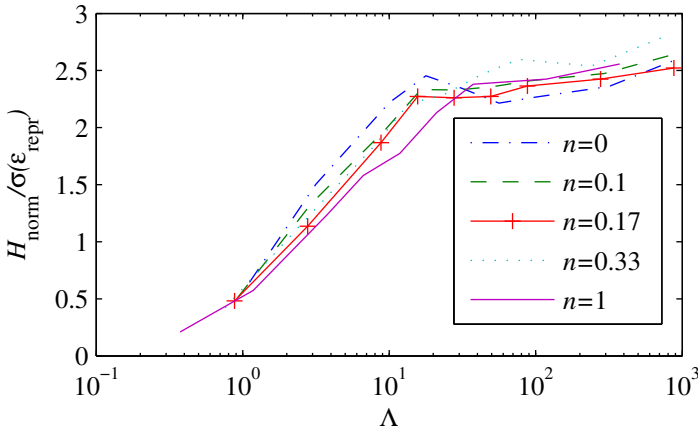


Figure 8. Scratch normal hardness divided by the yield stress at a plastic strain of 35 %, for different Λ ($\epsilon_{\text{repr}} = 35\%$) and n .

test is much less appropriate for standard material characterization, as will be discussed further below. Furthermore, the tangential hardness did not level out for large values of Λ (see Figure 9).

The scratch test is influenced by friction to a greater degree than is the standard indentation test. A numerical study was performed for $\Lambda(\epsilon_{\text{repr}} = 8\%) = 100$, investigating this effect. For this material the normal scratch hardness clearly decreased with increasing interfacial friction (see Figure 10). The opposite effect was noted for the tangential hardness (see Figure 11) This certainly complicates the interpretation of scratch experiments, particularly for material characterization based on the concept of a representative strain, since it is necessary to know both the dependence on friction and the coefficient of friction itself to draw any conclusion based on the scratch hardness. The representative level of plastic

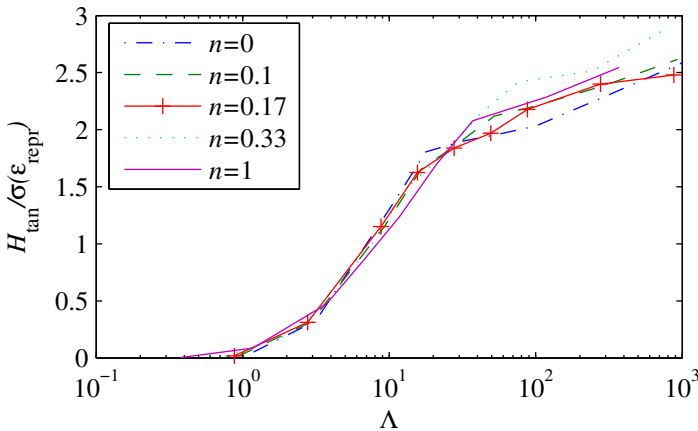


Figure 9. Scratch tangential hardness divided by the yield stress at a plastic strain of 35 % for different Λ ($\epsilon_{\text{repr}} = 35\%$) and n .

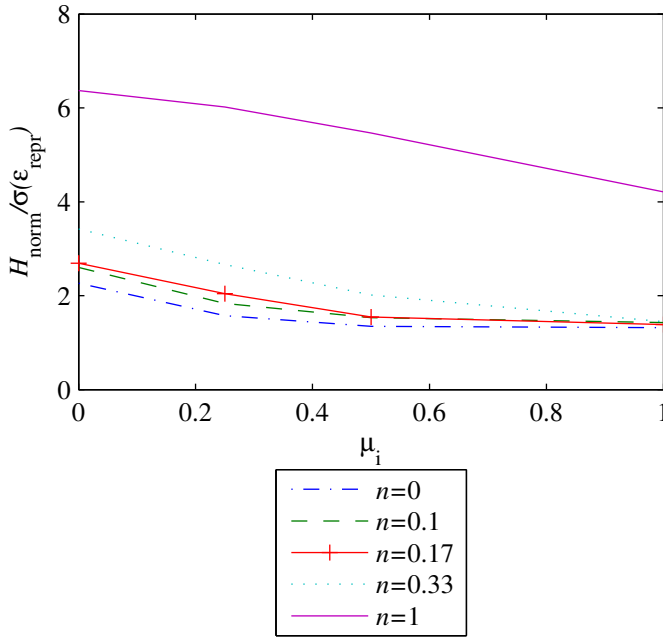


Figure 10. The influence of friction on normal hardness for strain hardening materials with different hardening n . Simulations with $\Lambda(\epsilon_{\text{repr}} = 8\%) = 100$.

strain varies with the coefficient of internal friction, which further complicates the matter. In fact, friction did increase ϵ_{repr} (for example, $\epsilon_{\text{repr}} \approx 0.5$ for $\mu_i = 0.2$) but it was still possible to determine accurate values for this variable. Interestingly, Felder and Bucaille [2006] find that the scratch hardness, when the contact area is calculated using Equation (10), is independent of the interfacial coefficient of friction. This feature was not studied in detail here, as a precise determination of the scratch width w was hard to achieve. However, preliminary results indicate that any frictional effect was within the margin of error.

Looking at the first principal stress distribution in Figures 17 and 18, it is clearly shown that the increasing shear exerted by the frictional force substantially increased the tensile forces in the wake of the stylus, potentially causing fracture.

It is also important to compare the values of the ratio of normal scratch hardness to tangential scratch hardness. This ratio may be expressed as

$$\frac{H_{\text{norm}}}{H_{\text{tan}}} = \frac{F_{\text{norm}} A_{\text{tan}}}{A_{\text{norm}} F_{\text{tan}}}. \quad (13)$$

The ratio $F_{\text{norm}}/F_{\text{tan}}$ may be replaced with $(\frac{2}{\pi} \tan \beta)^{-1}$ using Equation (17) below, assuming frictionless contact (see Section 4.3). The ratio of the tangentially projected area (A_{tan}) to the normally projected area (A_{norm}) can be written as

$$\frac{A_{\text{tan}}}{A_{\text{norm}}} = \frac{\frac{w^2}{4} \tan \beta}{(w/2)^2 \frac{\pi}{2}} = \frac{2}{\pi} \tan \beta \quad (14)$$

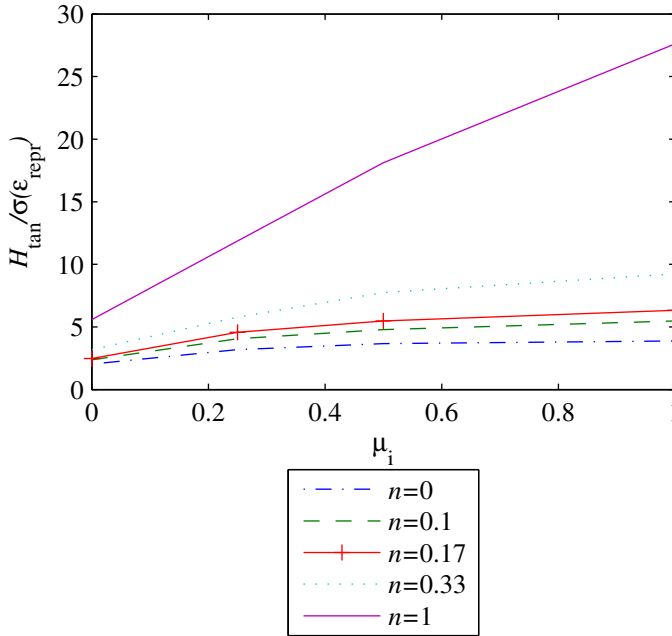


Figure 11. The influence of friction on tangential hardness for strain hardening materials with different hardening n . Simulations with $\Lambda(\epsilon_{repr} = 8\%) = 100$.

using Equation (10) and (11). Thus the hardness ratio simplifies to

$$\frac{H_{norm}}{H_{tan}} = \frac{\frac{2}{\pi} \tan \beta}{\frac{2}{\pi} \tan \beta} = 1. \tag{15}$$

This result can be seen in Figure 12, where the ratio of H_{norm}/H_{tan} goes to unity as the Johnson parameter Λ increases. For smaller Λ contact was no longer only on the front face and hence the ratio $H_{norm}/H_{tan} > 1$. This was due to the effect of the contact pressure on the rear face which decreases the tangential force F_{tan} , unlike the normal force F_{norm} which is increased by the contact force on the rear face. It is worth mentioning that Equation (15) applies to a conical stylus but not necessarily to styli of other shapes, since the derivation of Equation (15) relies on the independence of the contact pressure $p(r)$ from the angle φ [Subhash and Zhang 2002]. This is almost true for the conical stylus (as shown by the numerical calculations) but not necessarily for other shapes.

4.3. The apparent coefficient of friction. The tangential force divided by the normal force is known as the apparent coefficient of friction μ_0 or macroscopic friction at scratching. The apparent coefficient of friction is of interest since it will influence the amount of shear exerted on the specimen and consequently many other relevant scratch quantities.

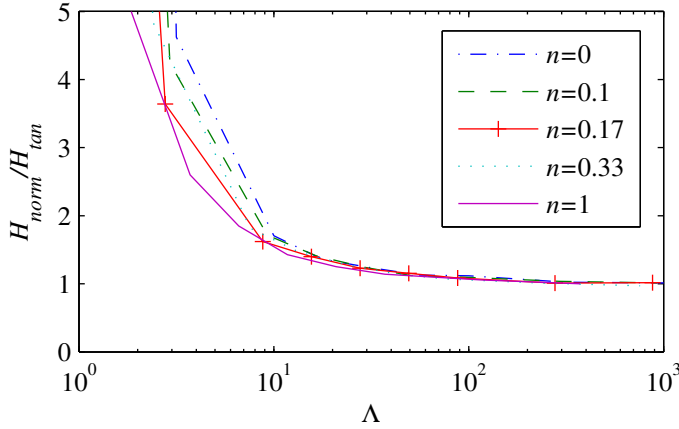


Figure 12. The ratio of normal hardness to tangential hardness at frictionless scratching. Note that the ratio goes to unity as Λ ($\epsilon_{\text{repr}} = 35\%$) increases.

The frictional force is often decomposed into an adhesive or interfacial part and a plowing part [Bowden and Tabor 1950]. This allows the apparent coefficient of friction μ_0 to be written as

$$\mu_0 = \mu_i + \mu_p, \tag{16}$$

where μ_i is the interfacial coefficient of friction, and μ_p is the plowing coefficient of friction. An estimate of the plowing coefficient of friction may be found by integrating the pressure vector over the surface. Assuming that the contact pressure is axi-symmetric over the contact area [Subhash and Zhang 2002] and that contact only occurs on the front face of the stylus with a constant contact radius [Goddard and Wilman 1962], the plowing coefficient of friction may be found by

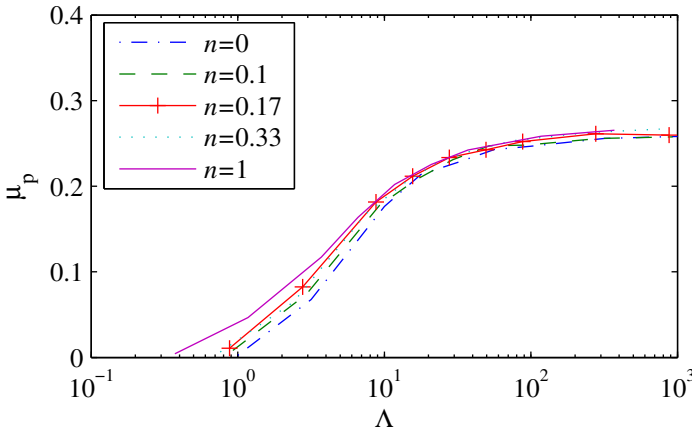


Figure 13. The plowing coefficient of friction. Λ is evaluated using $\epsilon_{\text{repr}} = 35\%$. Interfacial friction $\mu_i = 0$.

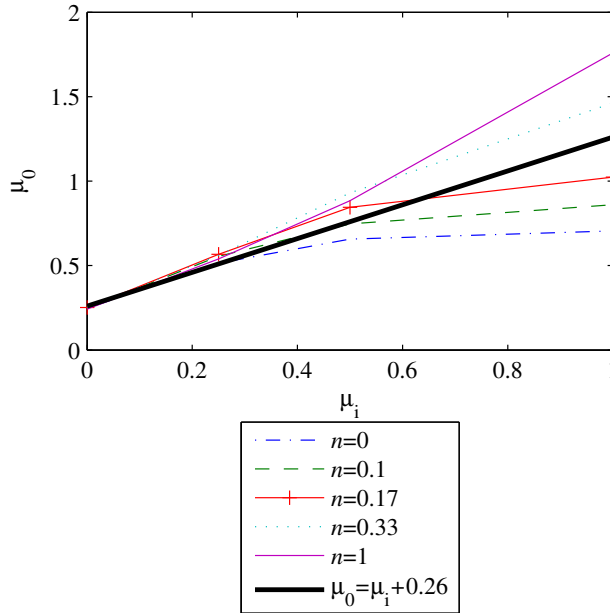


Figure 14. The apparent coefficient of friction μ_0 as a function of interfacial friction μ_i . Simulated with $n = 0, n = 0.1, n = 0.17, n = 0.33, n = 1$ and $\Lambda(\epsilon_{repr} = 8\%) = 100$. Equation (18) is plotted as a reference.

$$\mu_p = \frac{F_{tan}}{F_{norm}} = \frac{\mathbf{e}_t \cdot \int_A p(r) \mathbf{n} dA}{\mathbf{e}_n \cdot \int_A p(r) \mathbf{n} dA} = \tan(\beta) \frac{\int_A \cos(\varphi) p(r) dA}{\int_A p(r) dA} = \frac{2}{\pi} \tan \beta, \tag{17}$$

where $p(r)$ is the contact pressure, r is a radial coordinate, φ is the angle from the symmetry plane, $\mathbf{n} = (\sin(\beta) \cos(\varphi), \sin(\beta) \sin(\varphi), \cos \beta)$ is the surface normal vector, and \mathbf{e}_t and \mathbf{e}_n are vectors in the scratch direction and normal direction, respectively. Equation (17) gives $\mu_p \approx 0.26$ at frictionless contact for a cone with $\beta = 22^\circ$. Assuming a constant pressure distribution, Goddard and Wilman [1962] come to the same conclusion.

Previous simulations of frictionless scratching of elastic perfectly plastic materials ($n = 0$) show that the plowing coefficient of friction varies with Johnson’s parameter Λ [Bucaille et al. 2001]. In Figure 13 it can be seen that all materials (with different hardening exponents) follow the same master curve and that the plowing coefficient of friction levels out to an approximate value of 0.26, as predicted by Equation (17). Choosing a different ϵ_{repr} will only shift the curves along the x -axis. The coincidence of the curves in Figure 13 is, however, very robust with respect to the chosen representative strain. In fact, it is only the curve for $n = 1$ that was found to have a significant dependence on the chosen representative plastic strain.

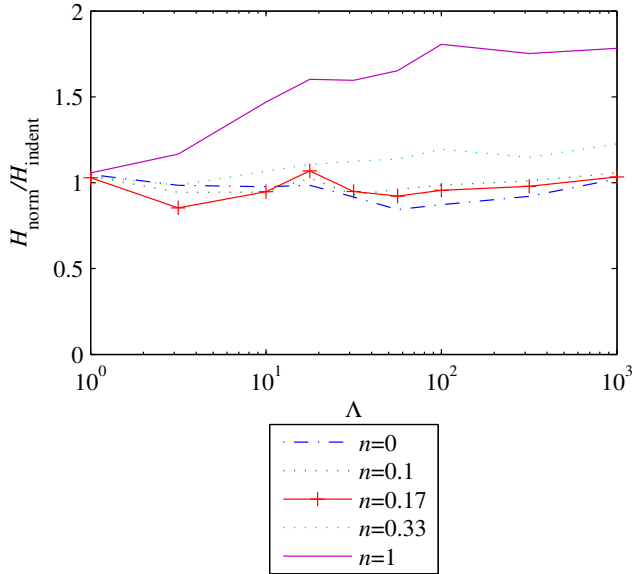


Figure 15. Ratio of scratch normal hardness to indentation hardness. Simulations with different n and Λ ($\epsilon_{\text{repr}} = 8\%$).

Such master curves could possibly be used for material characterization, in particular for polymers where Λ is small. It should be emphasized, though, that interfacial friction severely influences the apparent coefficient of friction, as shown in Figure 14. Thus it is of utmost importance to acquire an accurate value of the interfacial friction to be able to use the curve in Figure 13 for material characterization, which limits its practical usefulness.

To investigate the influence of hardening on the apparent coefficient of friction (when $\mu_i \neq 0$) a series of simulations for $\Lambda(\epsilon_{\text{repr}} = 8\%) = 100$ has been performed for a varying hardening parameter n . The results in Figure 14 show that for moderate levels of interfacial friction the apparent coefficient of friction μ_0 is independent of the hardening exponent n for nonfrictionless scratching. It is clear that this is not true for greater levels of interfacial friction. However, Figure 14 suggests that it is a reasonable approximation for the determination of the apparent coefficient of friction for levels of interfacial friction of up to 0.25. For materials with large Λ , where the plowing part of the apparent coefficient friction is constant (≈ 0.26 for a conical stylus with angle $\beta = 22^\circ$), Equation (16) may be simplified using Equation (17) to

$$\mu_0 = \mu_i + 0.26. \quad (18)$$

4.4. Scratch hardness vs. indentation hardness. The ratio of normal scratch hardness to normal indentation hardness is dependent on the hardening of the material in question. Since the scratch test is more sensitive to hardening than the indentation test, that is, has larger representative strain, a high level of hardening (n close to 1) gives a higher scratch hardness to indentation hardness ratio (see Figure 15). The opposite holds for low hardening or perfectly plastic materials. Thus for moderate levels of hardening the ratio of scratch normal hardness to indentation hardness is in the vicinity of 1. However, when interfacial

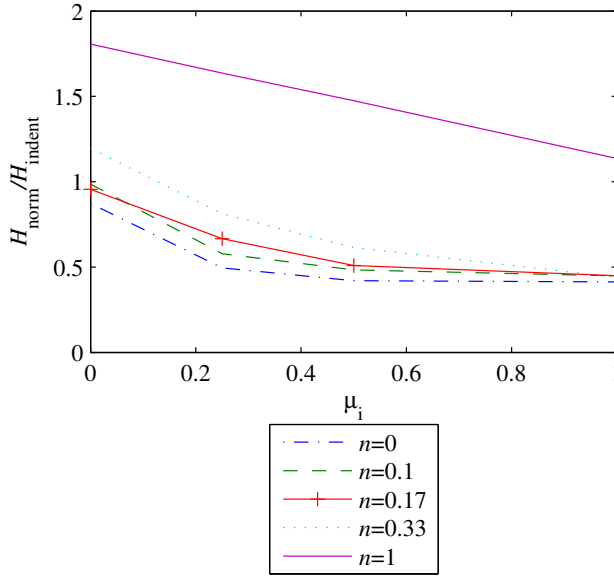


Figure 16. Ratio of scratch normal hardness to indentation hardness at varying interfacial friction μ_i . Simulations with different n and $\Lambda(\epsilon_{repr} = 8\%) = 100$.

friction was present as in Figure 16, the ratio of scratch normal hardness to indentation hardness was substantially decreased and no longer larger than 1.

The constant C in Figure 2 was, as stated earlier, found to be approximately 2.5 for scratching of predominately plastic materials. This is very close to the finding by Atkins and Tabor [1965] ($C \approx 2.54$) for conical indentation. However, it should be emphasized once again that the representative strain level is much higher at scratching (35% at scratching and 11% at indentation). This suggests that the ratio of scratch normal hardness to indentation hardness could simply be expressed as the ratio of the yield stress at 11% plastic strain to the yield stress at 35% plastic strain for materials undergoing mainly plastic deformation. However, this is not an exact relation, and in particular for higher levels of strain hardening this relation is not accurate.

It seems appropriate in this context to also discuss to some extent the behavior of field variables at scratching, particularly the stress fields, and specifically, to compare them to corresponding indentation quantities. In a practical situation this is pertinent to such features as crack initiation and growth, which are known to be of greater interest during scratching than during sharp (conical) indentation. In this discussion it is assumed in a straightforward manner that cracking is governed by a simple stress criterion such as

$$\sigma_1 = \sigma_B, \tag{19}$$

where σ_1 and σ_B are maximum principal stress and uniaxial failure stress, respectively. Accordingly, an approach based on fracture mechanics is not considered here.

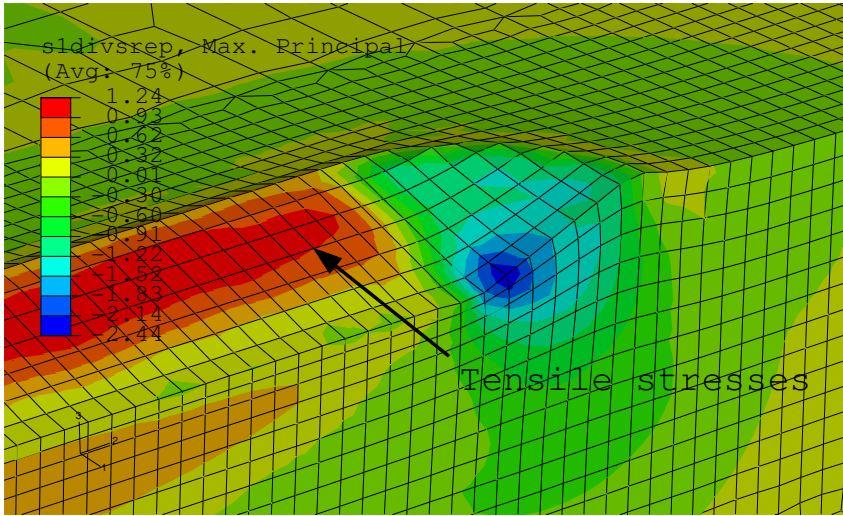


Figure 17. The first principal stress divided by the representative stress at frictionless scratching of a $\Lambda(\epsilon_{repr} = 8\%) = 100$ material with hardening exponent $n = 0.33$ and representative stress $\sigma(\epsilon_{repr} = 35\%) = 240$ MPa.

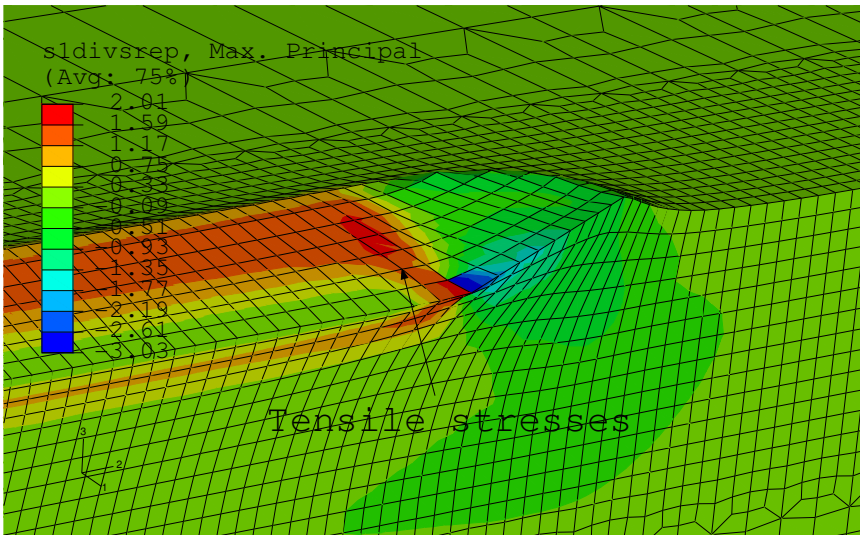


Figure 18. The first principal stress divided by the representative stress at scratching of a $\Lambda(\epsilon_{repr} = 8\%) = 100$ material with hardening exponent $n = 0.33$, representative stress $\sigma(\epsilon_{repr} = 35\%) = 240$ MPa and interfacial friction $\mu_i = 0.25$.

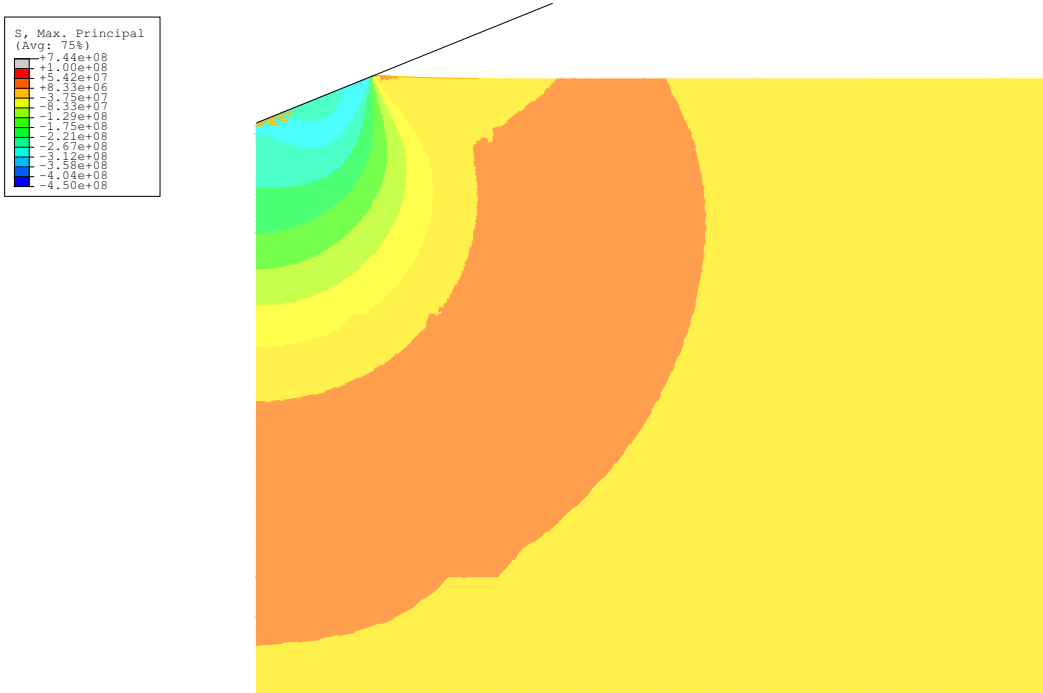


Figure 19. The first principal stress (in Pa) at frictionless indentation of a $\Lambda(\epsilon_{\text{repr}} = 8\%) = 100$ material with hardening exponent $n = 0.33$ and representative stress $\sigma(\epsilon_{\text{repr}} = 35\%) = 240$ MPa.

For this purpose, results for the maximum principal stress are shown for scratching in Figures 17 and 18, and for indentation in Figures 19 and 20, for frictionless as well as frictional contact ($\mu_i = 0.25$). The material in this case has a value of the Johnson parameter $\Lambda(\epsilon_{\text{repr}} = 8\%) = 100$, indicating mainly plastic but also some elastic deformation during scratching. As can be seen in Figures 17 and 18, the front of the stylus was exposed to compressive stresses during scratching as could be expected, while in the wake of the stylus, high tensile stresses developed, potentially causing fracture based on Equation (19). These tensile stresses substantially increased when frictional effects were accounted for, as shown in Figure 18.

In comparing the scratch results with corresponding indentation results, two features were immediately obvious from Figures 19 and 20. First, the tensile stresses at scratching were much higher than at indentation and, second, scratch values were much more influenced (that is, they increased) by friction. The same was also found, as indicated above, for global quantities such as hardness.

There are very few theoretical numerical studies concerned with the details of stress levels, specifically with cracking during scratching. However, recently Holmberg et al. [2003] presented a FEM study of scratching using a Rockwell indenter (a conical indenter with a spherical tip). In this study, scratching of a film/substrate system was considered (a single material combination, a TiN coating of a steel substrate, was explicitly investigated), which means that the present results and those of Holmberg et al. [2003] are not directly comparable. However, good qualitative agreement between the two sets of results are

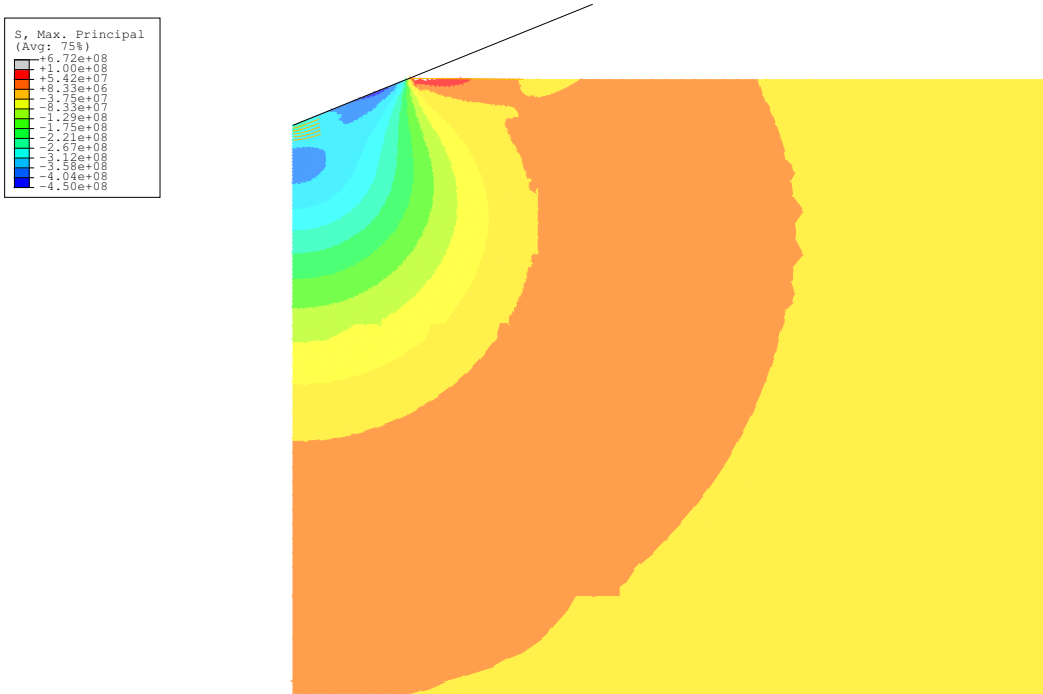


Figure 20. The first principal stress (in Pa) at indentation of a $\Lambda(\epsilon_{\text{repr}} = 8\%) = 100$ material with hardening exponent $n = 0.33$ and representative stress $\sigma(\epsilon_{\text{repr}} = 35\%) = 240$ MPa and interfacial friction $\mu_i = 0.25$.

found. For example, both investigations report a location of the maximum tensile stress in the wake of the stylus, which has also been noted in a number of previous studies.

5. Conclusions

The scratch test has been analyzed using a numerical approach based on the finite element method. The most important findings can be summarized as follows:

- The geometric approximation of the contact area given by Goddard and Wilman [1962] works well for materials where the plastic deformation is substantial. Not so, however, for materials with mainly elastic deformation.
- The concept of a representative strain holds true for scratching. The representative strain was found to be very large, approximately 35%.
- Interfacial friction will severely influence important scratch quantities.
- The numerical results suggest that other scratch quantities, such as the apparent coefficient of friction, can be used for material characterization.
- The normal scratch hardness and the tangential scratch hardness will be approximately equal for a conical stylus scratching a metallic material at low friction. As the friction increases this ratio will decrease since the normal hardness decreases and the tangential hardness increases.

- A useful first approximation of the apparent coefficient of friction can be found by adding the interfacial coefficient of friction to the master curve of friction (see Figure 13). For metallic materials this may be expressed as $\mu_0 = \mu_i + 0.26$. This explicit relation only holds for a conical stylus with angle $\beta = 22^\circ$. Obviously the opposite, to find the interfacial coefficient of friction μ_i from μ_0 , is also possible.
- The scratch normal hardness of a specimen is generally found to be equal to or higher than the indentation hardness of the same specimen, for frictionless contact. In case of a highly strain hardening material the scratch hardness will be substantially higher due to the much higher level of representative strain at scratching. Not so, however, when friction is present.

6. Acknowledgements

The authors wish to thank Professor Fred Nilsson for providing valuable advice and discussions, and for reading and commenting on the manuscript.

References

- [ABAQUS 2004] ABAQUS, *ABAQUS Manual v.6.4*, ABAQUS Inc., Pawtucket R.I. USA, 2004.
- [Atkins and Tabor 1965] A. G. Atkins and D. Tabor, "Plastic indentation in metals with cones", *Journal of The Mechanics and Physics of Solids* **13** (1965), 149–164.
- [Bowden and Tabor 1950] F. P. Bowden and D. Tabor, *The friction and lubrication of solids*, Clarendon press, 1950.
- [Briscoe et al. 1996] B. J. Briscoe, P. D. Evans, E. Pelillo, and S. K. Sinha, "Scratching maps for polymers", *Wear* **200** (1996), 137–147.
- [Bucaille et al. 2001] J. L. Bucaille, E. Felder, and G. Hochstetter, "Mechanical analysis of the scratch test on elastic and perfectly plastic materials with three-dimensional finite element modeling", *Wear* **249** (2001), 422–432.
- [Bucaille et al. 2004] J. L. Bucaille, E. Felder, and G. Hochstetter, "Experimental and three-dimensional finite element study of scratch test of polymers at large deformations", *Journal of Tribology* **126** (2004), 372–379.
- [Bull 1991] S. J. Bull, "Failure modes in scratch adhesion testing", *Surface and Coatings Technology* **50** (1991), 25–32.
- [Bull 1999] S. J. Bull, "Can scratch testing be used as a model for the abrasive wear of hard coatings?", *Wear* **233-235** (1999), 412–423.
- [Childs 1970] T. H. C. Childs, "The sliding of rigid cones over metals in high adhesion conditions", *International Journal of Mechanical Sciences* **12** (1970), 393–403.
- [Dao et al. 2001] M. Dao, N. Chollacoop, K. J. V. Vliet, T. A. Venkatesh, and S. Suresh, "Computational modeling of the forward and reverse problems in instrumented sharp indentation", *Acta Materialia* **49** (2001), 3899–3918.
- [Felder and Bucaille 2006] E. Felder and J. L. Bucaille, "Mechanical analysis of the scratching of metals and polymers with conical indenters at moderate and large strains", *Tribology International* **39** (2006), 70–87.
- [Fleck and Hutchinson 1993] N. A. Fleck and J. W. Hutchinson, "A phenomenological theory for strain gradient effects in plasticity", *Journal of the Mechanics and Physics of Solids, Volume* **41** (1993), 1825–1857.
- [Gauthier et al. 2001] C. Gauthier, S. Lafaye, and R. Schirrer, "Elastic recovery of a scratch in a polymeric surface: experiments and analysis", *Tribology International* **34** (2001), 469–479.
- [Giannakopoulos et al. 1994] A. E. Giannakopoulos, P.-L. Larsson, and R. Vestergaard, "Analysis of Vickers indentation", *International journal of Solids and Structures* **31** (1994), 2679–2708.
- [Gilormini and Felder 1983] P. Gilormini and E. Felder, "Theoretical and experimental study of the ploughing of a rigid-plastic semi-infinite body by a rigid pyramidal indenter", *Wear* **88** (1983), 195–206.
- [Goddard and Wilman 1962] J. Goddard and H. Wilman, "A theory of friction and wear during the abrasion of metals", *Wear* **5** (1962), 114–135.

- [Holmberg et al. 2003] K. Holmberg, A. Laukkanen, H. Ronkainen, K. Wallin, and S. Varjus, “A model for stresses, crack generation and fracture toughness calculation in scratched TiN-coated steel surfaces”, *Wear* **254** (2003), 278–291.
- [Johnson 1970] K. L. Johnson, “The correlation of indentation experiments”, *Journal of The Mechanics and Physics of Solids* **18** (1970), 115–126.
- [Johnson 1985] K. L. Johnson, *Contact mechanics*, Cambridge University Press, UK, 1985.
- [Larsson 2001] P.-L. Larsson, “Investigation of sharp contact at rigid-plastic conditions”, *International Journal of Mechanical Sciences* **43** (2001), 895–920.
- [Larsson et al. 1996] P.-L. Larsson, A. E. Giannakopoulos, E. Söderlund, D. J. Rowcliffe, and R. Vestergaard, “Analysis of Berkovich indentation”, *International Journal of Solids and Structures* **33** (1996), 221–248.
- [Laursen and Simo 1992] T. A. Laursen and J. C. Simo, “A study of microindentation using finite elements”, *Journal of Materials Research* **7** (1992), 618–626.
- [Malzbender and de With 2001] J. Malzbender and G. de With, “Analysis of scratch testing of organic-inorganic coatings on glass”, *Thin Solid Films* **386** (2001), 68–78.
- [Mata 2004] M. Mata, *Continuum analysis of sharp indentation experiments in metallic materials: theory and finite element simulations.*, Ph.D. thesis, Universitat Politècnica de Catalunya, 2004.
- [Subhash and Zhang 2002] G. Subhash and W. Zhang, “Investigation of the overall friction coefficient in single-pass scratch test”, *Wear* **252** (2002), 123–134.
- [Tabor 1951] D. Tabor, *Hardness of metals*, Cambridge University Press, UK, 1951.
- [Thouless 1998] M. D. Thouless, “An analysis of spalling in the microscratch test”, *Engineering Fracture Mechanics* **61** (1998), 75–81.
- [Vathaire et al. 1981] M. D. Vathaire, F. Delamare, and E. Felder, “An upper bound model of ploughing by a pyramidal indenter”, *Wear* **66** (1981), 55–64.
- [Wredenberg and Larsson 2005] F. Wredenberg and P.-L. Larsson, “Experimental and numerical analysis of the scratch test”, *WIT Transactions on Engineering Sciences* **49** (2005), 251–260.

Received 27 Sep 2006. Accepted 29 Nov 2006.

FREDRIK WREDENBERG: fredrik@hallf.kth.se
KTH Solid Mechanics, Royal Institute of Technology, S-10044, Stockholm, Sweden

PER-LENNART LARSSON: pelle@hallf.kth.se
KTH Solid Mechanics, Royal Institute of Technology, S-10044, Stockholm, Sweden